Journal of Sound and Vibration (1998) **213**(5), 889–906

DYNAMIC RESPONSE OF AN OVERHEAD CRANE SYSTEM

D. C. D. Oguamanam and J. S. Hansen

Institute for Aerospace Studies, University of Toronto, 4925 *Dufferin Street, Downsview, Ontario, Canada M3H 5T6*

AND

G. R. Heppler

Systems Design Engineering, University of Waterloo, Waterloo, Ontario, Canada N2L 3G1

(*Received* 24 *February* 1997, *and in final form* 3 *February* 1998)

A simply supported uniform Euler–Bernoulli beam carrying a crane (carriage and payload) is modelled. The crane carriage is modelled as a particle as is the payload which is assumed to be suspended from the carriage on a massless rigid rod and is restricted to motion in the plane defined by the beam axis and the gravity vector. The two coupled integro-differential equations of motion are derived using Hamilton's principle and operational calculus is used to determine the vibration of the beam which is, in turn, used to obtain the dynamics of the suspended payload. The natural frequencies of vibration of the beam–crane system for a stationary crane are investigated and the explicit frequency equation is derived for that set of cases. Numerical examples are presented which cover a range of carriage speeds, carriage masses, pendulum lengths and payload masses. It is observed that the location and the value of the maximum beam deflection for a given set of carriage and payload masses is dependent upon the carriage speed. At very fast carriage speeds, the maximum beam deflection occurs close to the end of the beam where the carriage stops as a result of inertial effects and at very slow speeds occurs near the middle of the beam because the system reduces to a quasi-static situation.

1. INTRODUCTION

The primary use of overhead cranes is in the transfer of "heavy" payloads from one location to another, thus they are found in areas such as airports, shipyards, and automobile plants. While the swing of the payload link poses an interesting control problem, a proper representation of the system dynamics is, in our view, an essential component in designing an effective controller.

The system reduces to an elastic beam with a moving load when the attachment to the payload—henceforth called a pendulum—is removed. This is a common feature in the design of railroads, highways, and bridges. While these are traditional civil engineering applications, the model is now used in ballistic machining problems, high-speed precision drilling, and problems involving two-phase flows [1–3].

One of the earliest studies on beams with moving load was done by Stokes [4] and the monograph by Frýba [5] is an excellent reference, with many analytical solution methods for simple cases. Lee [6] investigated the dynamic response of a beam with intermediate point constraints subjected to a moving load via the method of assumed modes. The point constraints were modelled as linear springs with stiffnesses of enough magnitude to guarantee a numerically zero deflection at these points. It was observed that the point

0022–460X/98/250889 + 18 $25.00/0/sv981564

constraints resulted in a significant reduction in the deflection of the beam for slow moving loads. The method of assumed modes was also used by Esmailzadeh and Ghorashi [7] to study the dynamic response of a single-span beam with a moving load that was caused by a uniform partially distributed moving mass. A similar analysis was implemented by Michaltsos *et al*. [8] with a concentrated moving load.

The application of the finite element method to the moving load problem can be found in references [3] and [9–11]. The study by Stanišić [12] is a departure from the aforementioned studies because the position of the moving load is included in the mode shapes derivation thus ensuring satisfaction of both the boundary and transient conditions. This technique is based on the use of operational calculus and was shown to exhibit fast convergence.

Khalily *et al*. [13] have used the technique by Stanišić [12] in modelling a cantilever beam with a moving mass. They showed that the inclusion of the position of the mass in the eigenfunctions provides superior results when compared with the conventional and more prevalent method in which the eigenfunctions are independent of the position of the mass.

This paper is an attempt to increase our understanding of the dynamics of an overhead crane system. We assume that the beam is simply supported and that it can be adequately modelled using Euler–Bernoulli beam theory. Further, we assume that the crane carriage transverses the beam at a known uniform speed and that the pendulum may be adequately modelled as a rigid massless bar. The motion of the pendulum is assumed to be planar with small angular displacements and displacement rates from the vertical.

A set of coupled, non-linear equations of motion is derived via Hamilton's principle. The complexity of these equations is increased by the presence of Dirac delta function terms. We obtain the transverse vibration of the beam using the method outlined in reference [12]. A polynomial is fitted to this result and then used to determine the dynamics of the pendulum. The effects of varying the various parameters are investigated.

2. DESCRIPTION OF THE SYSTEM

A schematic of the problem is depicted in Figure 1. An overhead crane carriage of mass m_c moves along the beam with a prescribed velocity $\dot{x}_c$. This implies that the position of the carriage is known at all times. A rigid rod of length L has one end attached to the carriage while the other end carries a payload of mass m_L. The rod is displaced from the vertical by angle θ.

The beam is simply supported and is assumed to be adequately modelled using Euler–Bernoulli beam theory. The properties of the beam are Young's modulus E, volume density ρ, cross-sectional area A, length L_b, and second moment of area I.

3. EQUATIONS OF MOTION

A dextral inertial frame $\mathscr{F}_a$ with basis vectors $\mathbf{a}_1$, $\mathbf{a}_2$, and $\mathbf{a}_3$ and co-ordinates xyz is attached at the left-hand end of the beam such that the $\mathbf{a}_1$ basis vector passes through the right-hand end of the beam and the $\mathbf{a}_2$ basis vector points in the direction of the static deflection as illustrated in Figure 1.

The position vector of an elemental mass of the beam $\mathbf{r}_b$, the position vector of the carriage $\mathbf{r}_c$, and the position vector of the load $\mathbf{r}_L$, can be expressed as

$$\mathbf{r}_b = x\mathbf{a}_1 + y(x, t)\mathbf{a}_2, \qquad \mathbf{r}_c = x_c(t)\mathbf{a}_1 + y(x_c, t)\mathbf{a}_2 \tag{1, 2}$$

and

$$\mathbf{r}_L = (x_c(t) + L_p \sin\theta)\mathbf{a}_1 + (y(x_c, t) + L_p \cos\theta)\mathbf{a}_2. \tag{3}$$

The corresponding velocities are

$$\dot{\mathbf{r}}_b = \frac{\partial y(x, t)}{\partial t}\,\mathbf{a}_2, \qquad \dot{\mathbf{r}}_c = \frac{\mathrm{d}x_c(t)}{\mathrm{d}t}\,\mathbf{a}_1 + \frac{\mathrm{d}y(x_c, t)}{\mathrm{d}t}\,\mathbf{a}_2 \tag{4, 5}$$

and

$$\dot{\mathbf{r}}_L = \left(\frac{\mathrm{d}x_c(t)}{\mathrm{d}t} + L_p \cos(\theta)\frac{\mathrm{d}\theta(t)}{\mathrm{d}t}\right)\mathbf{a}_1 + \left(\frac{\mathrm{d}y(x_c, t)}{\mathrm{d}t} - L_p \sin\theta\,\frac{\mathrm{d}\theta(t)}{\mathrm{d}t}\right)\mathbf{a}_2. \tag{6}$$

The kinetic energy of the system T is

$$T = T_b + T_c + T_L, \tag{7}$$

where

$$T_b = \tfrac{1}{2}\rho A \int_0^{L_b} \left(\frac{\partial y(x, t)}{\partial t}\right)^2 \mathrm{d}x, \qquad T_c = \tfrac{1}{2}m_c\left(\left(\frac{\mathrm{d}x_c(t)}{\mathrm{d}t}\right)^2 + \left(\frac{\mathrm{d}y(x_c, t)}{\mathrm{d}t}\right)^2\right), \tag{8, 9}$$

$$T_L = \tfrac{1}{2}m_L\left(\left(\frac{\mathrm{d}x_c(t)}{\mathrm{d}t}\right)^2 + 2L_p \cos\theta\,\frac{\mathrm{d}x_c(t)}{\mathrm{d}t}\,\frac{\mathrm{d}\theta(t)}{\mathrm{d}t} - 2L_p \sin\theta\,\frac{\mathrm{d}y(x_c, t)}{\mathrm{d}t}\,\frac{\mathrm{d}\theta(t)}{\mathrm{d}t}\right.$$

$$\left. + \left(\frac{\mathrm{d}y(x_c, t)}{\mathrm{d}t}\right)^2 + L_p^2\left(\frac{\mathrm{d}\theta(t)}{\mathrm{d}t}\right)^2\right). \tag{10}$$

The potential energy of the system U is

$$U = \tfrac{1}{2}EI \int_0^{L_b} \left(\frac{\partial y(x, t)}{\partial x}\right)^2 \mathrm{d}x - (m_c + m_L)gy(x_c, t) - m_L g L_p \cos\theta. \tag{11}$$

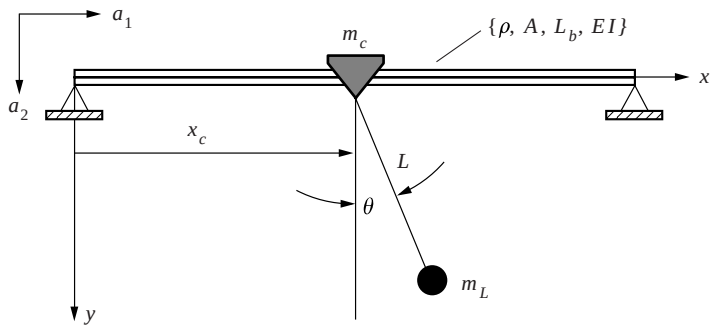

Figure 1. Schematic of the system.

Using T and U in Hamilton's principle and taking variations over $\theta(t)$ and $y(x, t)$ while observing their independence, we find the equations of motion, after some algebraic manipulations, to be

$$m_L L_p^2 \frac{\mathrm{d}^2\theta(t)}{\mathrm{d}t^2} + m_L L_p \cos\theta \frac{\mathrm{d}^2 x_c(t)}{\mathrm{d}t^2} - m_L L_p \sin\theta \frac{\mathrm{d}^2 y(x_c, t)}{\mathrm{d}t^2} + m_L g L_p \sin\theta = 0, \quad (12)$$

$$\int_0^{L_b} \left\{ \rho A \frac{\partial^2 y(x, t)}{\partial t^2} + EI \frac{\partial^4 y(x, t)}{\partial x^4} + (m_c + m_L)\left(\frac{\mathrm{d}^2 y(x, t)}{\mathrm{d}t^2} - g \right)\delta(x - x_c) \right.$$

$$\left. - m_L L_p \left(\sin\theta \frac{\mathrm{d}^2\theta(t)}{\mathrm{d}t^2} + \cos(\theta)\left(\frac{\mathrm{d}\theta(t)}{\mathrm{d}t} \right)^2 \right)\delta(x - x_c) \right\} \mathrm{d}x = 0, \quad (13)$$

with the boundary conditions

$$y(0, t) = \frac{\partial^2 y(0, t)}{\partial x^2} = y(L_b, t) = \frac{\partial^2 y(L_b, t)}{\partial x^2} = 0 \quad (14)$$

and initial conditions

$$y(x, 0) = \frac{\partial y(x, 0)}{\partial t} = \frac{\mathrm{d}\theta(0)}{\mathrm{d}t} = x_c(0) = 0 \qquad \text{and} \qquad \theta(0) = \theta_0. \quad (15)$$

In the simple case where one has a simply supported beam with a mass fixed somewhere in the span one can find that the governing frequency equation is

$$\frac{\beta m}{\rho A} (\sin(\beta L_b)(\cosh(\beta(L_1 - L_2)) - \cosh(\beta L_b)) + \sinh(\beta L_b)(\cos(\beta(L_1 - L_2)) - \cos(\beta L_b))) - 4 \sin(\beta L_b) \sinh(\beta L_b) = 0, \quad (16)$$

where L_1 is the position of the mass as measured from the left end of the beam where $x = 0$. The other parameters in equation (16) are defined as

$$\beta^4 = \frac{\omega^2 \rho A}{EI}, \qquad L_b = L_1 + L_2 \quad \text{and} \quad m = m_c + m_L.$$

This relation ignores the motion of the payload and treats the carriage and payload as a single point mass. It may be observed that in the event that $m = 0$, $L_1 = 0$ or $L_2 = 0$, equation (16) reduces to the frequency equation for a uniform simply supported beam,

$$\sin(\beta L_b) = 0.$$

3.1. NON-DIMENSIONALIZED EQUATIONS OF MOTION

To obtain the non-dimensionalized forms of the equations of motion, equations (12) and (13), we follow Stanišić [12] and define

$$v(\xi, t) = \frac{y(x, t)}{L_b}, \qquad \xi = \frac{x}{L_b}, \qquad \xi_c(t) = \frac{x_c(t)}{L_b}, \qquad \varepsilon_1 = \frac{m_c}{\rho A L_b},$$

$$\varepsilon_2 = \frac{m_L}{\rho A L_b}, \qquad t = \alpha\tau, \qquad \alpha^2 = \frac{\rho A L_b^4}{EI}, \qquad \varepsilon = \varepsilon_1 + \varepsilon_2, \quad (17)$$

$$p_1 = \frac{m_c g L_b^2}{EI}, \qquad p_2 = \frac{m_L g L_b^2}{EI}, \qquad p = p_1 + p_2, \qquad L = \frac{L_p}{L_b}.$$

Using the above definitions, the non-dimensional form of equation (12) can be written as

$$\varepsilon_2 L \frac{\mathrm{d}^2\theta(\tau)}{\mathrm{d}\tau^2} + \varepsilon_2 \cos\theta \frac{\mathrm{d}^2\xi_c(\tau)}{\mathrm{d}\tau^2} - \varepsilon_2 \sin\theta \frac{\mathrm{d}^2 v(\xi_c, \tau)}{\mathrm{d}\tau^2} + p_2 \sin\theta = 0 \tag{18}$$

and that of equation (13) as

$$\int_0^1 \left\{ \frac{\partial^2 v(\xi, \tau)}{\partial\tau^2} + \frac{\partial^4 v(\xi, \tau)}{\partial\xi^4} + \varepsilon \frac{\mathrm{d}^2 v(\xi_c, \tau)}{\mathrm{d}\tau^2} \delta(\xi - \xi_c) \right.$$

$$\left. - \left(\xi\varepsilon_2 \left(\sin\theta \frac{\mathrm{d}^2\theta(\tau)}{\mathrm{d}\tau^2} - \cos(\theta) \left(\frac{\mathrm{d}\theta(\tau)}{\mathrm{d}\tau} \right)^2 \right) + p \right) \delta(\xi - \xi_c) \right\} \mathrm{d}\xi = 0. \tag{19}$$

The corresponding non-dimensionalized boundary conditions are

$$v(0, \tau) = \frac{\partial^2 v(0, \tau)}{\partial\xi^2} = v(1, \tau) = \frac{\partial^2 v(1, \tau)}{\partial\xi^2} = 0 \tag{20}$$

and the non-dimensionalized initial conditions are

$$v(\xi, 0) = \frac{\partial v(\xi, 0)}{\partial\tau} = \frac{\mathrm{d}\theta(0)}{\mathrm{d}\tau} = 0 \qquad \text{and} \qquad \theta(0) = \theta_0. \tag{21}$$

The non-dimensional form of the frequency equation given in equation (16) is

$$\begin{aligned} \lambda\varepsilon(&\sin(\lambda)(\cosh(\lambda(2\xi_c - 1)) - \cosh(\lambda)) \\ &+ \sinh(\lambda)(\cos(\lambda(2\xi_c - 1)) - \cos(\lambda))) \\ &- 4\sin(\lambda)\sinh(\lambda) = 0, \end{aligned} \tag{22}$$

with $\sin(\lambda) = 0$ corresponding to the frequency equation for a uniform simply supported beam.

4. SOLUTION METHOD

If we assume a crane carriage speed $\dot{\xi}_c$ = constant and also assume that $\theta(\tau)$ and $\mathrm{d}\theta(\tau)/\mathrm{d}\tau$ are small and that their products are negligible, then the non-dimensionalized equations of motion can be written as

$$\frac{\mathrm{d}^2\theta(\tau)}{\mathrm{d}\tau^2} - \left(\frac{1}{L} \frac{\mathrm{d}^2 v(\xi_c, \tau)}{\mathrm{d}\tau^2} - \alpha^2 \frac{g}{L_p} \right) \theta(\tau) = 0 \tag{23}$$

and

$$\int_0^1 \left(\frac{\partial^2 v(\xi, \tau)}{\partial\tau^2} + \frac{\partial^4 v(\xi, \tau)}{\partial\xi^4} + \varepsilon \frac{\mathrm{d}^2 v(\xi, \tau)}{\mathrm{d}\tau^2} \delta(\xi - \xi_c) - p\delta(\xi - \xi_c) \right) \mathrm{d}\xi = 0. \tag{24}$$

The use of the small angle and small angular rate assumption allows the uncoupling of the beam motion from the payload motion but not conversely. Except for the simplifications enjoyed as a result of this assumption the governing equations remain non-linear coupled integro-differential equations. Equation (23) could result in a Hill–Mathieu equation under some conditions and this would imply the possibility of an "unstable" motion. Note that equation (24) is identical to equation (5) in reference [12]

without the spring term. Thus, one can follow reference [12] and derive an approximate solution for the vibration of the beam. The actual derivation process is very lengthy and tedious and will not be repeated here, instead, the reader is urged to consult Stanišić [12] for more details.

Assume a separable solution to equation (24) in the form

$$v(\xi, \tau) = V(\xi)\, \mathrm{e}^{\mathrm{j}\Omega\tau}, \tag{25}$$

where Ω is a non-dimensional frequency. Using this expression, the following frequency equation results [12]:

$$\sin(\lambda)\sinh(\lambda) + \frac{\varepsilon}{2}\lambda(\sin(\lambda(\xi_c - 1))\sin(\lambda\xi_c)\sinh(\lambda) - \sinh(\lambda(\xi_c - 1))\sinh(\lambda\xi_c)\sin(\lambda)) = 0, \tag{26}$$

where $\lambda^2 = \Omega$. The orthonormalized eigenfunction is expressed as

$$V_n(\xi, \xi_c) = \frac{1}{\sqrt{B_n(\xi_c)}} \begin{cases} \Psi_{n_L}(\xi, \xi_c - 1), & 0 \leqslant \xi < \xi_c, \\ \Psi_{n_R}(\xi - 1, \xi_c), & \xi_c < \xi \leqslant 1, \end{cases} \tag{27}$$

where

$$\Psi_{n_L}(\xi, \xi_c - 1) = \sin(\lambda_n\xi)\sin(\lambda_n(\xi_c - 1))\sinh(\lambda_n) - \sinh(\lambda_n\xi)\sinh(\lambda_n(\xi_c - 1))\sin(\lambda_n), \tag{28}$$

$$\Psi_{n_R}(\xi - 1, \xi_c) = \sin(\lambda_n(\xi - 1)\sin(\lambda_n\xi_c)\sinh(\lambda_n) - \sinh(\lambda_n(\xi - 1))\sinh(\lambda_n\xi_c)\sin(\lambda_n) \tag{29}$$

and

$$B_n(\xi_c) = 2\sin(\lambda_n)\sinh(\lambda_n(3\Psi_n(\xi_c) - \xi_c|\Psi'_{n_L}(\xi_c) + \Psi'_{n_R}(\xi_c)|)) + 2\lambda_n(\sin^2(\lambda_n\xi_c)\sinh^2(\lambda_n) - \sinh^2(\lambda_n\xi_c)\sin^2(\lambda_n)) + \varepsilon\Psi_n^2(\xi_c). \tag{30}$$

The solution to equation (24) can be expressed as a summation of the product of the orthonormal eigenfunctions $V_m(\xi, \xi_c)$ and undetermined coefficients $q_m(\tau, \xi_c)$ such that

$$v(\xi, \tau) = \sum_{m=1}^{\infty} V_m(\xi, \xi_c) q_m(\tau, \xi_c). \tag{31}$$

It was assumed earlier that the carriage travels with a constant velocity. Now, it is also assumed that the expressions $\partial V_m(\xi, \xi_c)/\partial\xi_c$ and $\partial q_m(\xi_c, \tau)/\partial\xi_c$ and their second derivatives are small enough that their products can be ignored when compared with $(\partial^2 q_m(\xi_c, \tau)/\partial\tau^2)V_m(\xi, \xi_c)$ [12]. Thus,

$$\frac{\partial^2}{\partial\tau^2}(V_m(\xi, \xi_c)q_m(\xi_c, \tau)) \approx \frac{\partial^2 q_m(\xi_c, \tau)}{\partial\tau^2} V_m(\xi, \xi_c). \tag{32}$$

Substituting equation (31) into equation (24) and using equation (32), the following equation results after some algebraic manipulations:

$$\frac{\partial^2 q_m(\xi_c, \tau)}{\partial\tau^2} + \lambda_m^4(\xi_c)q_m(\xi_c, \tau) = pV_m(\xi_c, \xi_c), \tag{33}$$

TABLE 1

Material properties

Parameter	Value
ρ	$8{\cdot}0 \times 10^3\ \mathrm{kgm}^{-3}$
E	$2{\cdot}117 \times 10^{11}\ \mathrm{Pa}$
L_b	$10{\cdot}0\ \mathrm{m}$
A	$16{\cdot}0 \times 10^{-4}\ \mathrm{m}^2$
I	$2{\cdot}13 \times 10^{-7}\ \mathrm{m}^4$
g	$9{\cdot}81\ \mathrm{ms}^{-2}$
$\rho A L_b$	128 kg
α	1·685

with initial conditions

$$q_m(0, \xi_c) = \dot{q}_m(0, \xi_c) = 0. \tag{34}$$

The following is the solution to the above equation which is obtained from operational calculus [14]:

$$q_m(\tau, \xi_c) = p \int_0^\tau (\tau - \phi) V_m(\xi_c(\phi), \xi_c(\phi))\, \mathrm{d}\phi$$

$$- \int_0^\tau (\tau - \phi) \lambda_m^4(\xi_c(\phi)) q_m(\phi, \xi_c(\phi))\, \mathrm{d}\phi. \tag{35}$$

Equation (35) is substituted into equation (31) to determine the beam deflection under the carriage $v(\xi_c, \tau)$. A Chybeshev polynomial series is then fitted to the resulting beam deflections and its second derivative is used in equation (23) to numerically obtain the dynamics of the payload.

5. NUMERICAL EXAMPLES

The beam is assumed to be square in cross-section and to be made of steel with the material properties outlined in Table 1. The crane carriage travels from one end of the beam to the other in all simulations. Before investigating the dynamics of the pendulum our analysis is validated by simulating the dynamics of the beam. In particular we seek to reproduce Figure 4 in reference [12].

The ratio of the mass of the carriage to the mass of beam ε_1 is varied over the values 0·0, 0·05, and 0·10, the ratio of the mass of the payload to the mass of the beam is fixed at $\varepsilon_2 = 0{\cdot}15$, and the ratio of the length of the pendulum to the length of the beam is fixed at $L = 0{\cdot}15$. The simulation is carried out for three constant carriage speeds $\dot{\xi}_c = 0{\cdot}5$, 1·0 and $2{\cdot}0\ \mathrm{s}^{-1}$.

Before considering the cases where the carriage and payload are moving, it is instructive to first consider the natural frequencies of the beam when the carriage and payload are stationary. The purpose of this preliminary investigation into the frequency behaviour of the system for stationary masses is to demonstrate the complexity of the behaviour even in this simple scenario. Careful examination of equation (22) reveals that when the mass is positioned at $\xi = k/n$, $k = 0, 1, 2, \ldots, n$ of the span, (i.e., at the modal nodes) the natural frequency of mode n is identical to the natural frequency of the same mode in the

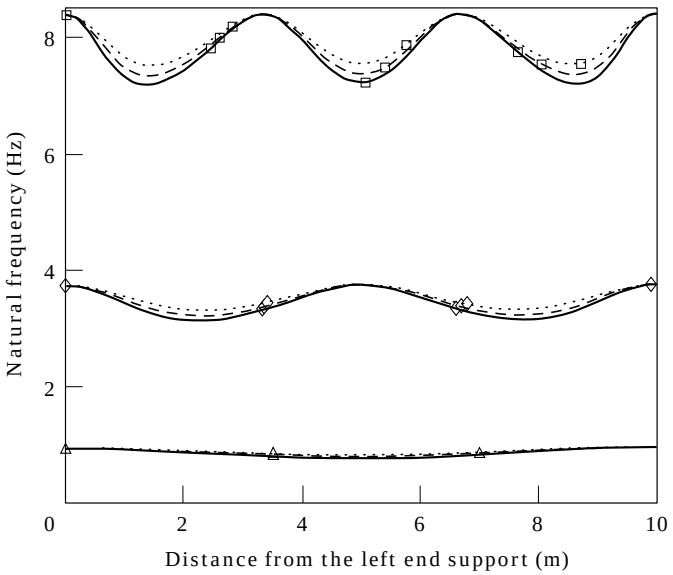

Figure 2. Natural frequencies of a beam with a fixed mass in the span for $\varepsilon = 0{\cdot}15$ ($\cdots$), $0{\cdot}20$ (——), $0{\cdot}25$; (——); △, 1st mode; ◇, 2nd mode; □, 3rd mode.

case where there is no mass on the beam. This is illustrated in Figure 2 for the first three natural frequencies. The material and geometric properties used to produce this figure are given in Table 1.

As expected, the addition of the mass in the span of the beam decreases the natural frequency of the system, except as noted above, and the larger the mass the greater the decrease. The location of the minima in Figure 2 is dependent not only on the size of the

TABLE 2

Stationary mass, ω_1 Hz

ξ_c	$\varepsilon = 0{\cdot}15$	$\varepsilon = 0{\cdot}20$	$\varepsilon = 0{\cdot}25$
0·000	0·9323203	0·9323203	0·9323203
0·500	**0·8173761**	**0·7874778**	**0·7606099**
1·000	0·9323203	0·9323203	0·9323203

TABLE 3

Stationary mass, ω_2 Hz

ξ_c	$\varepsilon = 0{\cdot}15$	$\varepsilon = 0{\cdot}20$	$\varepsilon = 0{\cdot}25$
0·000	3·7292810	3·7292810	3·7292810
0·225	3·3111085	3·2133922	**3·1296904**
0·230	3·3103962	**3·2133021**	3·1303428
0·235	**3·3103629**	3·2139979	3·1318551
0·500	3·7292810	3·7292810	3·7292810
0·765	**3·3103629**	3·2139979	3·1318551
0·770	3·3103962	**3·2133021**	3·1303428
0·775	3·3111085	3·2133922	**3·1296904**
1·000	3·7292810	3·7292810	3·7292810

TABLE 4

Stationary mass, ω_3 Hz

ξ_c	$\varepsilon = 0{\cdot}15$	$\varepsilon = 0{\cdot}20$	$\varepsilon = 0{\cdot}25$
0·000	8·3908824	8·3908824	8·3908824
0·135	7·5320338	7·3458314	**7·1927402**
0·140	7·5263722	**7·3431626**	7·1935066
0·145	**7·5240848**	7·3442846	7·1982738
0·333	8·3908824	8·3908824	8·3908824
0·500	**7·5381336**	**7·3657407**	**7·2245910**
0·666	8·3908824	8·3908824	8·3908824
0·855	**7·5240848**	7·3442846	7·1982738
0·860	7·5263722	**7·3431626**	7·1935066
0·865	7·5320338	7·3458314	**7·1927402**
1·000	8·3908824	8·3908824	8·3908824

mass but also on the position of the mass as may be seen in the data presented in Tables 2–4 where the local minimum values are in bold. Of interest here is that, in the third mode data, the global minimum does not occur when the mass is at midspan.

Figure 3 depicts the beam deflection under the carriage as the carriage travels at $\dot{\xi}_c = 0{\cdot}5\ \mathrm{s}^{-1}$. It is observed that the magnitude of the maximum deflection increases with the mass of the carriage. This is to be expected given the higher gravitational loads associated with the greater masses. It may further be observed in Figure 3 that for the lower values of ε_1 (i.e., 0·0 and 0·05) the maximum deflection occurs at or very near to the midspan of the beam but for the larger carriage mass ($\varepsilon_1 = 0{\cdot}1$) the peak deflection under the carriage definitely occurs past the middle of the beam.

This effect is accentuated in Figures 4 and 5 where results for the same system, but with the carriage speed increased from $\dot{\xi}_c = 0{\cdot}5$ to 1·0 and $2{\cdot}0\ \mathrm{s}^{-1}$, respectively, are illustrated Here it may be observed that the location of the maximum deflection (under the carriage) has moved forward, away from the middle of the beam to the right; the higher the carriage speed, the further the maximum is moved to the right. This is caused by a coupling of the

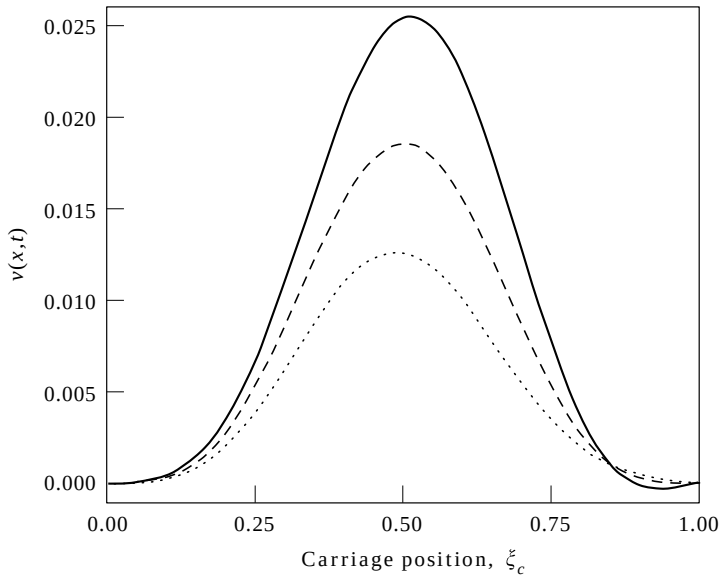

Figure 3. Beam deflection under the carriage for $\dot{\xi}_c = 0{\cdot}5\ \mathrm{s}^{-1}$ and $\varepsilon_2 = 0{\cdot}15$; · · · · , $\varepsilon_1 = 0$; ——, 0·05; ——, 0·10.

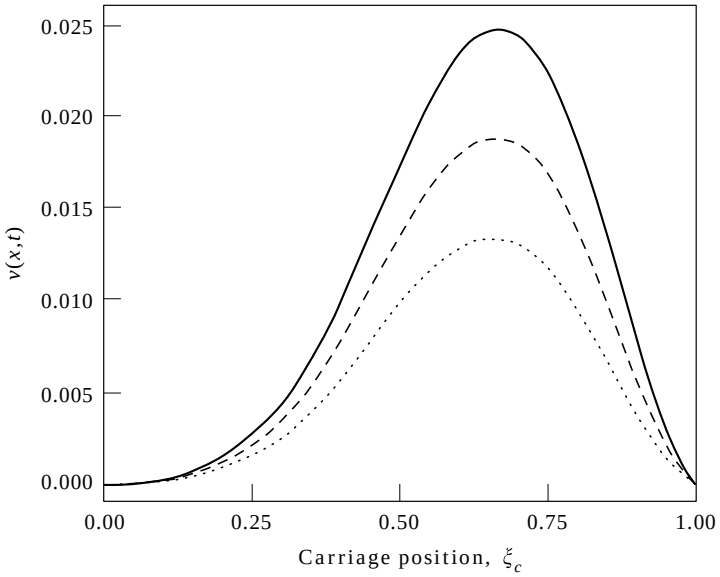

Figure 4. Beam deflection under the carriage for $\dot{\xi}_c = 1{\cdot}0\ \mathrm{s}^{-1}$ and $\varepsilon_2 = 0{\cdot}15$; · · · · , $\varepsilon_1 = 0$; ——, 0·05; ——, 0·10.

beam motion and the motion of the carriage. Because the beam motion is dynamic it is vibrating as the crane carriage advances and when the speed of the carriage is sufficiently large it can reach a point on the beam that is more than half way across before a constructive superposition of the gravitational loading and the beam motion combine to yield a maximum deflection under the carriage. Figures 3 and 4 demonstrate that this effect is more sensitive to changes in carriage speed than it is to changes in the carriage mass. It may also be noted in Figure 4 that, just as in the previous case, the magnitude of the maximum deflection increases with the mass of the carriage.

Further, upon close examination of Figures 4 and 5 it may be noted that the magnitude of the various maxima is lower than their corresponding values for a carriage speed of $0{\cdot}5\ \mathrm{s}^{-1}$. This is due to the increased speed of the carriage and can be appreciated by considering the two limiting cases of $\dot{\xi}_c \to 0$ and $\dot{\xi}_c \to \infty$. In the former limit we approach a sequence of quasi-static loadings where at each instant the maximum deflection of the beam is under the carriage and dynamic effects are negligible. In the later limit the beam would not deflect at all due to inertial effects and the negligible transit time.

With reference to Figure 4 the ($\varepsilon_1 = 0{\cdot}05$, $\varepsilon_2 = 0{\cdot}15$) combination is the nearest to, and is in close agreement with, the scenario presented in Stanišić [12].

5.1. PAYLOAD DYNAMICS

The vibration of the pendulum carrying the payload is examined under three different scenarios to determine the effect of the length of the pendulum, the effect of the mass of the carriage and the mass of the payload, and finally, the effect of the carriage speed.

5.1.1. *Case* 1: *effect of the pendulum length*

To examine the effect of the length of the pendulum a carriage speed $\dot{\xi}_c$ of $1{\cdot}0\ \mathrm{s}^{-1}$, a carriage mass to beam mass ratio ε_1 of 0·05 and a payload mass to beam mass ratio $\varepsilon_2 = 0{\cdot}15$ are used. The results are depicted in Figure 6 where a definite change in frequency is evident. While the payload is suspended from a moving carriage it is, by virtue of the constant carriage velocity, in an inertial frame (ignoring the transverse acceleration of the

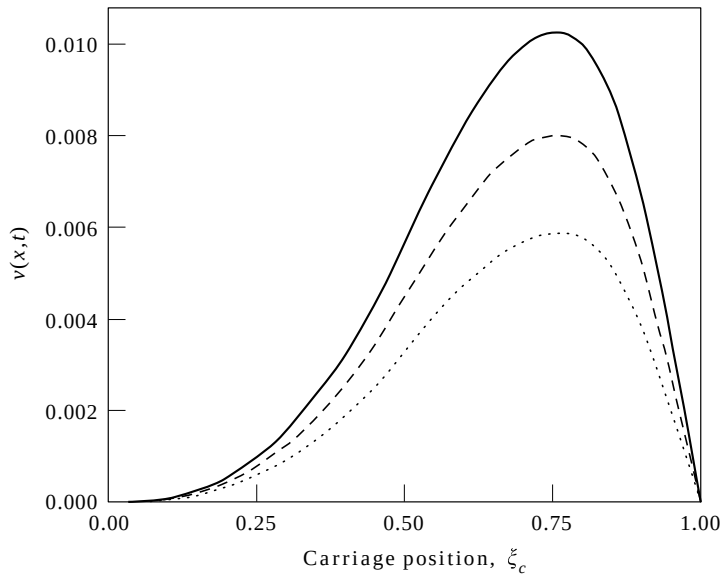

Figure 5. Beam deflection under the carriage for $\dot{\xi}_c = 2{\cdot}0\ \mathrm{s}^{-1}$ and $\varepsilon_2 = 0{\cdot}15$; · · · · , $\varepsilon_1 = 0$; ——, 0·05; ——, 0·10.

beam) and should behave just as a stationary pendulum would. Figure 6 shows that, as expected, the swing frequency is inversely proportional to the square root of the length of the pendulum and, for this example, the beam vibration has no discernible effect on the payload motion as compared to changes in the pendulum length.

5.1.2. *Case* 2: *effect of carriage mass*

In this example the ratio of the length of the pendulum to the length of the beam L, the ratio of the payload mass to the beam mass ε_2, and the carriage speed $\dot{\xi}_c$ are each fixed at 0·10, 0·15, and $1{\cdot}0\ \mathrm{s}^{-1}$, respectively, while the ratio of the mass of the carriage to the

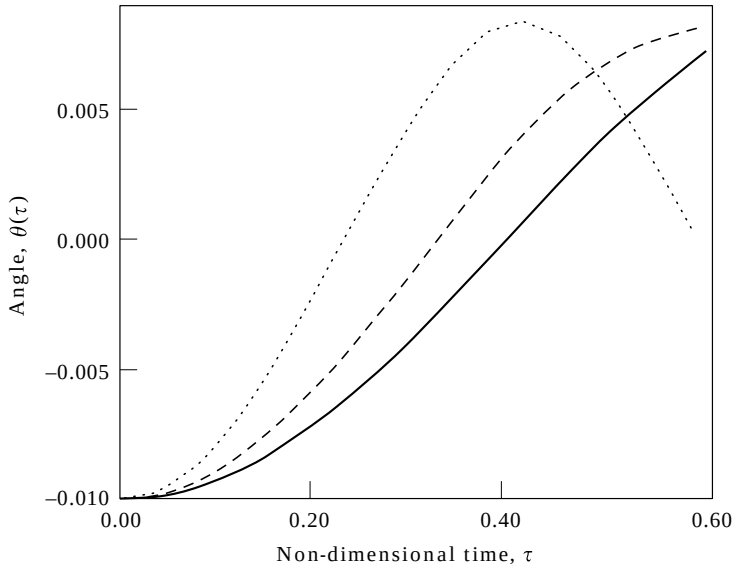

Figure 6. Effect of the pendulum length: · · · · , $L = 0{\cdot}05$; ——, 0·10; ——, 0·15.

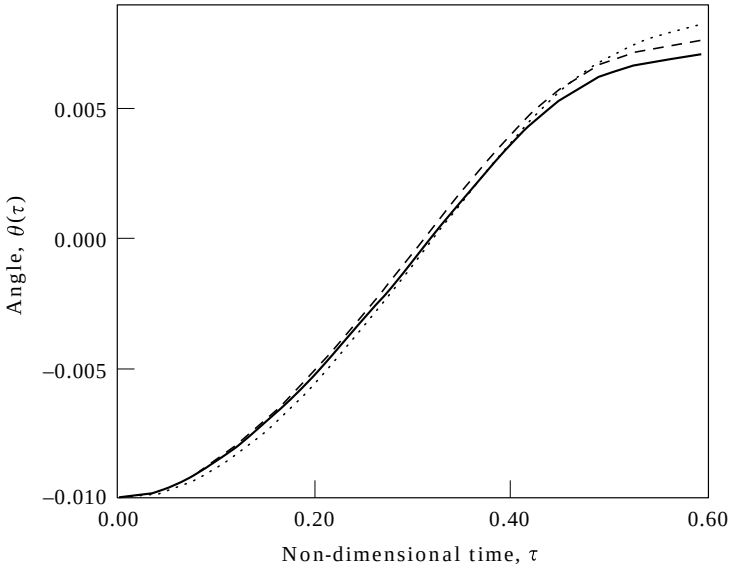

Figure 7. Effect of carriage mass: · · · · , $\varepsilon_1 = 0{\cdot}05$; ––, 0·10; ——, 0·15.

mass of the beam ε_1 is varied as 0·05, 0·10 and 0·15. The swing angle versus non-dimensional time is plotted in Figure 7 for each ε_1.

The beam motion and carriage mass contribute an effective stiffness coupling term to the dynamics of the pendulum as can be seen by considering the leading factor of the penultimate term in equation (23), i.e., the factor

$$\frac{\mathrm{d}^2 v(\xi_c, \tau)}{\mathrm{d}\tau^2} \tag{36}$$

which also appears in the beam equation (24) with ε as a leading factor. The plots do not reveal any apparent change in the swinging frequency of the pendulum but, the magnitude of the swing of the pendulum increases slightly with decreasing carriage mass.

From the equations of motion, equations (23) and (24), it is expected that for fixed values of ε a variation in the mass of the payload would give the same effect as a variation in the mass of the carriage. Thus, that situation will not be considered explicitly.

5.1.3. *Case* 3: *effect of carriage speed*

Here, the ratio of the carriage mass to the beam mass, the ratio of the payload mass to the beam mass, and the ratio of the pendulum length to the beam length are fixed at $\varepsilon_1 = 0{\cdot}05$, $\varepsilon_2 = 0{\cdot}15$ and $L = 0{\cdot}10$, respectively, while the carriage speed is varied as $\dot{\xi}_c = 0{\cdot}2$, 0·5 and 1·0 s^{-1}. The results are illustrated in Figures 8–10.

The non-dimensional terminating time τ_* for each speed is determined according to

$$\tau_* = \frac{t_*}{\alpha} = \frac{L_b}{\alpha \dot{x}_c} = \frac{1}{\dot{x}_c L_b} \sqrt{\frac{EI}{\rho A}}.$$

These plots are not presented in the same figure because the time window that is available for the pendulum to swing is different for each carriage speed—it increases with decreasing carriage speed. Thus, a full cycle is observed at the lowest speed because the period is smaller than the total travel time of the carriage.

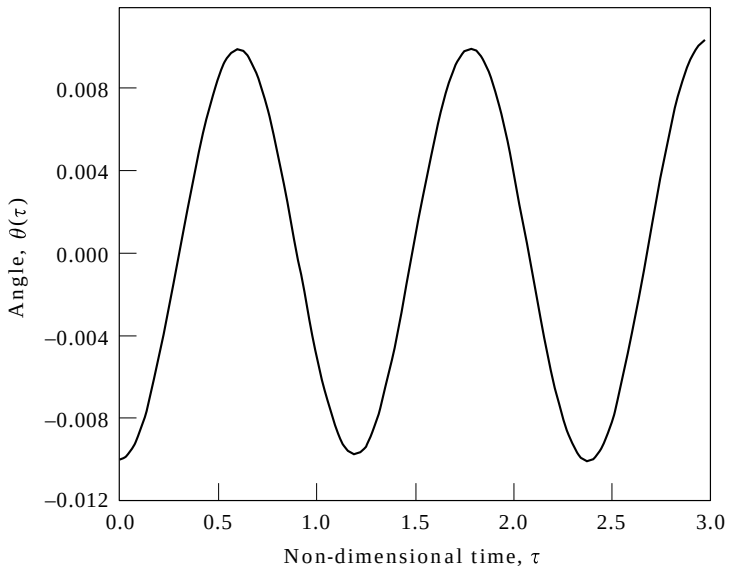

Figure 8. Effect of carriage speed for $\varepsilon_1 = 0{\cdot}05$, $\varepsilon_2 = 0{\cdot}15$, $L = 0{\cdot}10$ and $\dot{\xi}_c = 0{\cdot}2\ \mathrm{s}^{-1}$.

The results at the slowest speed (Figure 8) is of particular interest in that the amplitude of vibration starts to slowly grow after about $\tau = 2{\cdot}0$. Figure 9 shows that the pendulum completes one-half period by the time the carriage reaches the end of the beam when the carriage speed is $0{\cdot}5\ \mathrm{s}^{-1}$ while a quarter period is observed at a carriage speed of $1{\cdot}0\ \mathrm{s}^{-1}$ (Figure 10).

To further improve our understanding of the effects of the carriage speed on the pendulum motion, Figure 11 has been included which depicts the beam transverse deflection under the carriage. These plots are similar to those of Figures 3–5 but for fixed carriage and payload masses and varied carriage speeds. Taking the results depicted in

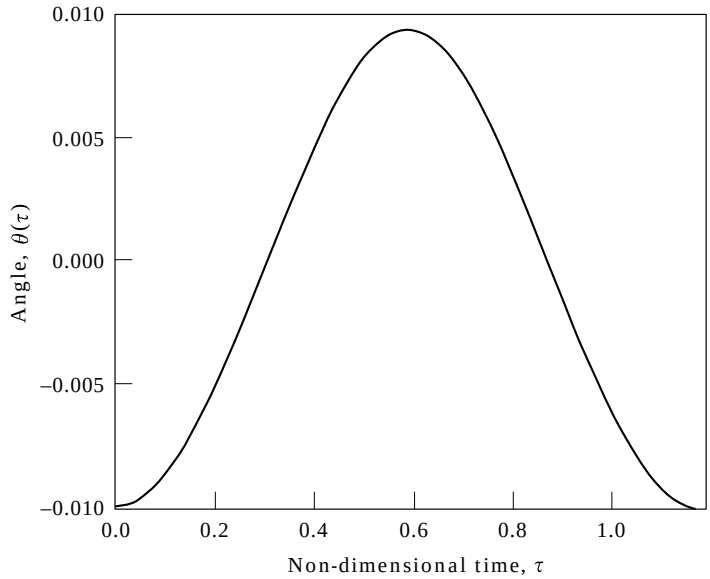

Figure 9. Effect of carriage speed for $\varepsilon_1 = 0{\cdot}05$, $\varepsilon_2 = 0{\cdot}15$, $L = 0{\cdot}10$ and $\dot{\xi}_c = 0{\cdot}5\ \mathrm{s}^{-1}$.

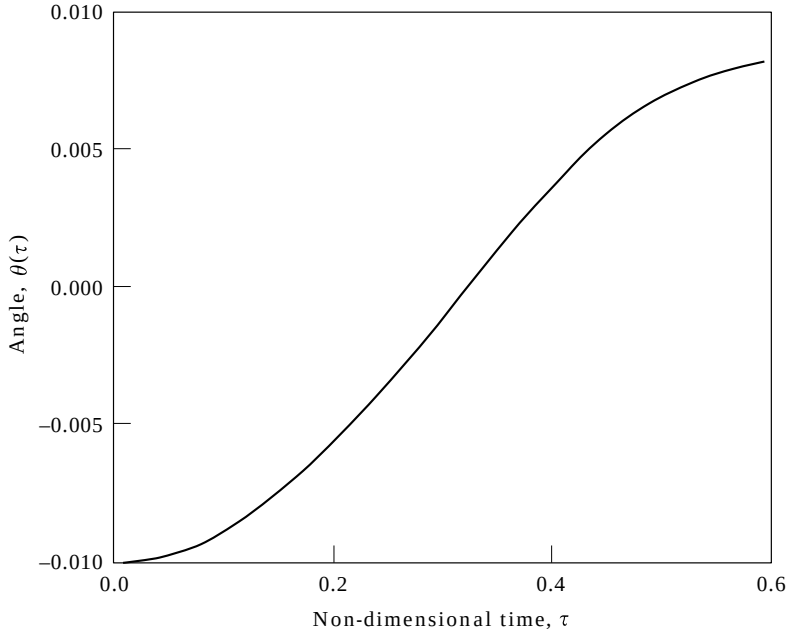

Figure 10. Effect of carriage speed for $\varepsilon_1 = 0{\cdot}05$, $\varepsilon_2 = 0{\cdot}15$, $L = 0{\cdot}10$ and $\dot{\xi}_c = 1{\cdot}0\ \mathrm{s}^{-1}$.

Figures 3–5 into consideration, one can conclude that there is a threshold carriage speed that will generate beam deflections under the carriage that are symmetric about the middle of the beam.

What the above suggests is that the location and the value of the maximum beam deflection for a given set of carriage and payload masses is dependent upon the carriage speed. At very fast carriage speeds, the maximum beam deflection is expected to occur close to the end of the beam where the carriage stops because in those cases the deflections are

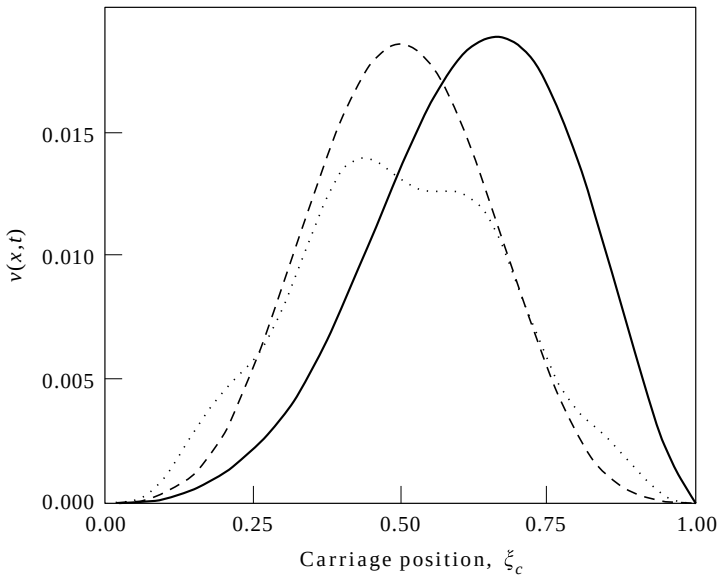

Figure 11. Beam deflection under the carriage for $\varepsilon_1 = 0{\cdot}05$, $\varepsilon_2 = 0{\cdot}15$ and $L = 0{\cdot}10$; · · · · , $\dot{\xi}_c = 0{\cdot}2\ \mathrm{s}^{-1}$; ——, $0{\cdot}5\ \mathrm{s}^{-1}$; ——, $1{\cdot}0\ \mathrm{s}^{-1}$.

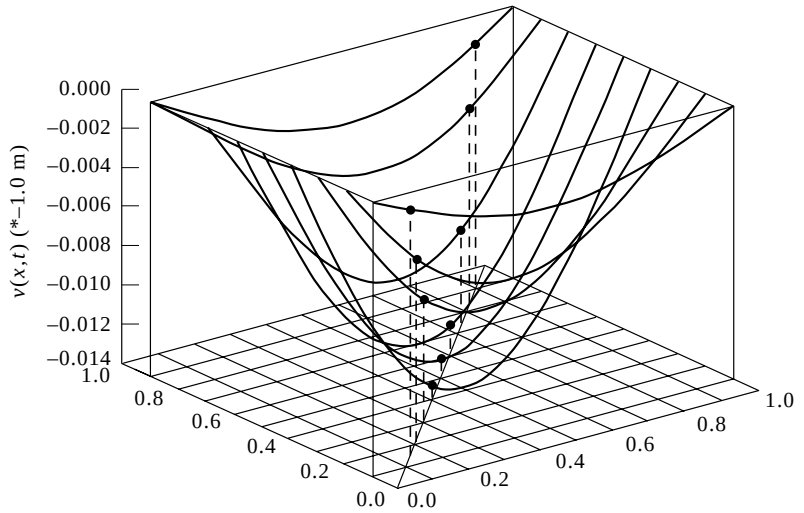

Figure 12. Beam deflection for a given carriage location for $\varepsilon_1 = 0{\cdot}05$, $\varepsilon_2 = 0{\cdot}15$, $L = 0{\cdot}10$ and $\dot{\xi}_c = 0{\cdot}2\ \mathrm{s}^{-1}$ (time = 5·0 s, beam length = 10·0 m).

dominated by inertial effects. At very slow speeds, the maximum beam deflection is expected to occur at the middle of the beam because the system reduces to a quasi-static situation. With regard to the slow speeds, it is observed that the maximum beam deflection occurs before the middle of the beam within a particular range of carriage speeds. This may be explained by noting that the beam vibration frequency is varying because of the variation in mass distribution. An analytical deduction of this range of carriage speeds for a given configuration is difficult, if not impossible.

Plots of the beam deflection history for a carriage speed of 2 m/s over a 10-m long beam are presented in Figure 12. This figure is presented to provide a qualitative understanding of the interaction between the carriage speed and beam vibration frequency. The negative of the deflections has been plotted for aesthetic reasons because the reference frame of the beam was positioned in such a manner that downward deflections of the beam were positive.

Each curve in the figure is a beam deflection profile traced when the carriage has travelled along the beam for a particular time. The dots represent the carriage location at time intervals of 0·5 s as it traverses the beam. The diagonal line at the bottom of the figure is the projection of the carriage trajectory in the time–position plane. In a like manner the plot for a carriage speed of $0{\cdot}2\ \mathrm{s}^{-1}$ in Figure 11 is the projection of the carriage trajectory onto the beam deflection–time plane for this same example.

The beam deflection profile traced when the carriage has travelled 4 m along the beam provides the maximum beam deflection for all the profiles. Note, however, that this maximum deflection does not occur under the carriage but rather at a point forward of the carriage. If one considered the beam as simply supported without any concentrated load, the period for the ith mode is

$$T_i = \frac{2}{i^2\pi}\left(\frac{\rho A L^4}{EI}\right)^{1/2} = \frac{2\alpha}{i^2\pi}.$$

From Figure 2 it can be seen that, for the first mode, this will yield a reasonably close estimate for the dominant period.

The period of the first mode of the beam is 1·0726 s and the carriage will travel 4·29 m after $2T_1$ periods which correlates very well with the maximum deflection under the carriage at the slowest carriage speed ($\dot{\xi} = 0{\cdot}2\ \mathrm{s}^{-1}$) in Figure 11. The other local peaks in that figure occur at $1T_1$, $3T_1$ and $4T_1$ periods indicating that this carriage speed is sufficiently slow to allow the beam vibrations to be observed in the response. At the next higher carriage speed, i.e., $\dot{\xi} = 0{\cdot}5\ \mathrm{s}^{-1}$ the peak beam deflection under the carriage occurs at a location (time) that corresponds very closely to $1T_1$ period. The peak displacement under the carriage for the highest carriage speed reported in Figure 11 does not correlate with an integer multiple of T_1 or, apparently, any other system characteristic period.

6. SUMMARY

The dynamics of an overhead crane system with the carriage moving at a specified constant speed has been examined. The beam portion of the crane was modelled as an Euler–Bernoulli beam, the carriage as a particle and the pendulum as a rigid massless rod with a particle tip mass. The coupled integro-differential equations of motion were derived using Hamilton's principle.

Our assumption of a small angle of rotation (or swing) of the pendulum has led to a system of equations in which the dynamics of the pendulum are dependent on the dynamics of the beam but not the converse. Allowing a large angular displacement of the pendulum would introduce a bidirectional coupling between the beam and the pendulum and introduce the possibility of pendulum instability due to the flexible support offered by the beam; this would be a worthwhile area for future inquiry. The acceleration of the beam under the carriage acts as an effective stiffness contribution in the governing equation of motion of the pendulum but this effect is not unidirectional since the term can take either positive or negative values and hence the pendulum acts as if it has a time varying stiffness coefficient.

The mode shapes of the beam were determined as functions of the instantaneous location of the carriage on the beam. The vibration of the beam was determined via operational calculus and fitted to a Chybeshev polynomial series. The resulting expression was then used to simulate the dynamics of the pendulum.

The results obtained from the numerical calculations that employed the non-dimensional formulation of the problem indicate that the deflection of the beam is dependent on both the carriage speed and the mass of the combined carriage and payload mass. In particular, the magnitude of the deflection increases with increasing crane mass at all carriage speeds. For a given crane mass, there is a threshold carriage speed at which the beam deflection under the carriage is symmetric about the middle of the beam. The position of the maximum deflection tends to drift to the right or the left of the beam centre depending on whether the operating speed is above or below this threshold. Further, the magnitude of the maximum deflection tends to decrease with increasing drift from symmetry.

The threshold speed and the location of the maximum beam deflection for a given carriage speed are observed to be functions of the beam vibration frequency due to what may be considered as constructive interference between the gravitational deflection of the beam and the vibrational behaviour of the beam. The value of the maximum beam deflection for a given set of carriage and payload masses is dependent upon the carriage speed. For high carriage speeds, the maximum beam deflection occurs close to the end of the beam where the carriage stops because the deflections are dominated by inertial effects of the carriage. At very slow speeds the beam behaves in a quasi-static manner and the maximum beam deflection occurs close to the middle of the beam.

The dynamics of the pendulum are dependent on the carriage mass, the payload mass, the length of the pendulum, and the carriage speed. The carriage mass or payload mass effect is reflected in the magnitude of the vibration while changes in the pendulum length affect both the frequency and magnitude of the swing.

Finally, an unstable pendulum swing is possible at some carriage speeds and configurations because the governing equation will reduce to a Hill–Mathieu equation.

REFERENCES

1. F. Hara 1976 *Transactions of the JSME* **42**, 2400–2411. Two-phase flow induced vibration in a horizontal piping system.
2. R. Katz, C. W. Lee, A. G. Ulsoy and R. A. Scott 1987 *ASME Journal of Vibration, Acoustics, Stress and Reliability in Design* **109**, 361–365. Dynamic stability and response of a beam subject to a deflection dependent moving load.
3. Y. H. Lin and M. W. Trethewey 1990 *Journal of Sound and Vibration* **136**, 323–342. Finite element analysis of elastic beams subjected to moving dynamic loads.
4. G. G. Stokes 1849 *Transactions of the Cambridge Philosophical Society*, Part 5, 707–735. Discussion of a differential equation relating to the breaking of railway bridges.
5. L. Frýba 1972 *Vibration of Solids and Structures under Moving Loads*. Groningen: Noordhoff.
6. H. P. Lee 1994 *Journal of Sound and Vibration* **171**, 369–395. Dynamic response of a beam with intermediate point constraints subject to a moving load.
7. E. Esmailzadeh and M. Ghorashi 1995 *Journal of Sound and Vibration* **184**, 9–17. Vibration analysis of beams traversed by uniform partially distributed moving masses.
8. G. Michaltsos, D. Sophianopoulos and A. N. Kounadis 1996 *Journal of Sound and Vibration* **191**, 357–362. The effect of a moving mass and other parameters on the dynamic response of a simply supported beam.
9. J. Hino, T. Yoshimura and N. Ananthanarayana 1985 *Journal of Sound and Vibration* **100**, 477–491. Vibration analysis of non-linear beams subjected to a moving load using the finite element method.
10. T. Yoshimura, J. Hino and N. Ananthanarayana 1985 *Journal of Sound and Vibration* **104**, 179–186. Vibration analysis of non-linear beams subjected to a moving load by using the Galerkin method.
11. M. Olsson 1991 *Journal of Sound and Vibration* **145**, 299–307. On the fundamental moving load problem.
12. M. M. Stanišić 1985 *Ingenieur-Archiv* **55**, 176–185. On a new theory of the dynamic behavior of the structures carrying moving masses.
13. F. Khalily, M. F. Golnaraghi and G. R. Heppler 1994 *Nonlinear Dynamics* **5**, 493–513. On the dynamic behavior of a flexible beam carrying a moving mass.
14. B. Friedman 1956 *Principles and Techniques of Applied Mathematics*. New York: John Wiley and Sons.

APPENDIX: NOMENCLATURE

A	beam cross-sectional area
E	Young's modulus
I	second moment of the area
L	ratio of the length of the pendulum to the length of the beam
L_b	length of the beam
L_p	length of the pendulum
m_c	mass of the carriage
m_L	mass of the payload
p	summation of non-dimensional carriage and payload weights
p_1	non-dimensional weight of the carriage
p_2	non-dimensional weight of the payload
q_m	undetermined coefficients
$\mathbf{r}_b$	position vector of an elemental mass
$\mathbf{r}_c$	position vector of the carriage

$\mathbf{r}_L$	position vector of the payload
t	time
T	system kinetic energy
V_m	orthonormal eigenfunctions
U	system potential energy
$v(\xi, \tau)$	non-dimensional transverse displacement
x	co-ordinate of the beam
x_c	position of the carriage on the beam
$y(x, t)$	transverse displacement
α	natural frequency constant of the beam
δW	system virtual work
ε	summation of the non-dimensional carriage and payload masses
ε_1	non-dimensional mass of the carriage
ε_2	non-dimensional mass of the payload
θ	pendulum angle from the vertical
λ	square of the non-dimensional frequency
ξ	non-dimensional co-ordinate of the beam
ξ_c	non-dimensional position of the carriage
ρ	volume mass density
τ	non-dimensional time
Ω	non-dimensional frequency
$\dot{(\,)}$	time derivative
$(\,)'$	spatial derivative